

<https://helda.helsinki.fi>

Pure and Sb-doped ZrO₂ for removal of IO₃⁻ from radioactive waste solutions

Suorsa, V.

2022

Suorsa, V., Otaki, M., Virkanen, J. & Koivula, R. 2022, 'Pure and Sb-doped ZrO₂ for removal of IO₃⁻ from radioactive waste solutions', *International Journal of Environmental Science and Technology*, vol. 19, pp. 5155-5166. <https://doi.org/10.1007/s13762-021-03487-9>

<http://hdl.handle.net/10138/354564>

<https://doi.org/10.1007/s13762-021-03487-9>

cc_by

publishedVersion

Downloaded from Helda, University of Helsinki institutional repository.

This is an electronic reprint of the original article.

This reprint may differ from the original in pagination and typographic detail.

Please cite the original version.



Pure and Sb-doped ZrO_2 for removal of IO_3^- from radioactive waste solutions

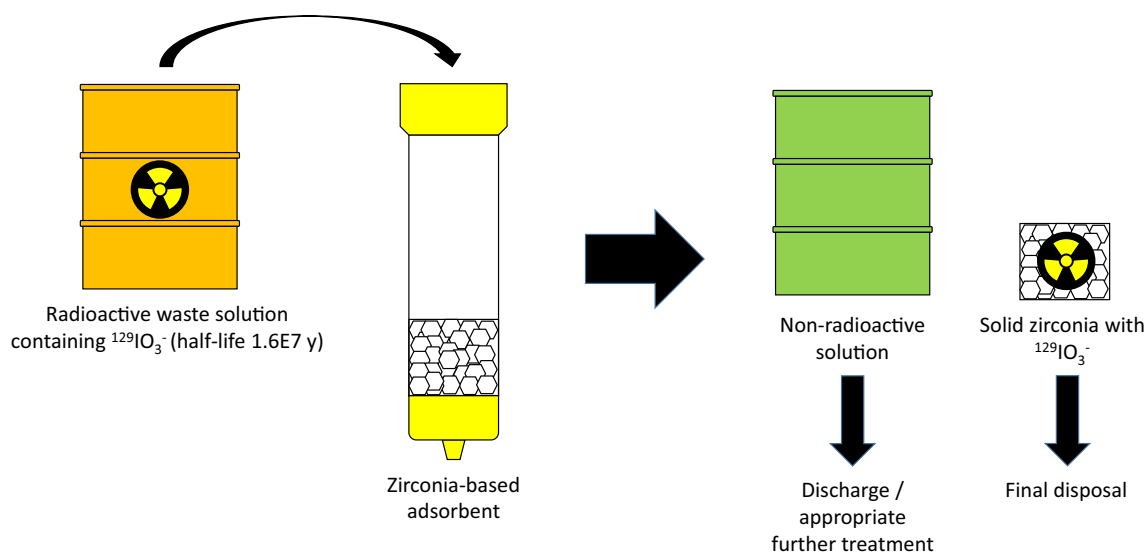
V. Suorsa¹ · M. Otaki¹ · J. Virkanen² · R. Koivula¹

Received: 2 February 2021 / Revised: 22 April 2021 / Accepted: 11 June 2021
© The Author(s) 2021

Abstract

Radioactive ^{129}I with a long half-life (1.57×10^7 y) and high mobility is a serious radiohazard and one of the top risk radionuclides associated with its accidental and planned releases to nature. The complex speciation chemistry of iodine makes its removal a complicated task, and usually a single method is not able to remove all iodine species. Especially its oxidized form iodate (IO_3^-) lacks a selective and effective removal method. Here, the granular aggregates of hydrous zirconium oxides with and without antimony doping were tested for IO_3^- removal and the effects of contact time, competing anions in different concentrations and pH were examined. The materials showed high selectivity for IO_3^- (K_d over up to 50,000 ml/g) in the presence of competing ions and relatively fast uptake kinetics (eq. < 1 h). However, $\text{B}(\text{OH})_4^-$ and SO_4^{2-} , as competing ions, lowered the iodate uptake significantly in basic and acidic solution, respectively. The suitability of the materials for practical applications was tested in a series of column experiments where the materials showed remarkably high apparent capacity for the IO_3^- uptake (3.2–3.5 mmol/g).

Graphic abstract



Keywords Iodate removal · ^{129}I · Zirconium oxide · Anion uptake · Decontamination

Editorial responsibility: Samareh Mirkia.

✉ V. Suorsa
valteri.suorsa@helsinki.fi

Extended author information available on the last page of the article

Published online: 23 June 2021



Springer

Introduction

Iodine is a vital element for mammals as it is a critical component of hormones produced in a thyroid gland. The insufficient supply of iodine has several harmful health effects which are all together described as the iodine deficiency disorders (Zimmermann and Andersson 2012; Zimmermann and Boelaert 2015). In order to eliminate the adverse health effects of iodine deficiency, serious efforts have been put in action worldwide to supply the populations with the vital iodine (Andersson et al. 2010).

However, in addition to the stable isotope ^{127}I , the thyroid gland absorbs the radioactive iodine isotopes generated by nuclear fission reaction. This increases the absorbed radiation dose of the gland which leads to an elevated risk of thyroid cancer. Iodine has several radioactive isotopes from which the short-lived isotopes, e.g. ^{131}I ($t_{1/2} = 8$ d) or ^{133}I ($t_{1/2} = 20.8$ h), pose an acute risk in the case of a nuclear accident, whereas the long-term significance comes from ^{129}I with an extremely long half-life (1.57×10^7 y). Indeed, the nuclear accidents at Chernobyl and Fukushima released large amounts of ^{129}I to the environment (Aldahan et al. 2007; Hou et al. 2009, 2013). To minimize the internal dose of population, the authorities have set national or global guidance levels for the concentration of ^{129}I (WHO: 1 Bq/L (World Health Organization 2017); DWS in USA 0.04 Bq/L (Kaplan et al. 2014)) in drinking water. In the case of elevated concentrations, the purification of the water is required (Li et al. 2018).

Because of the potential radiation dose to populations, efficient treatment materials and methods are required for iodine containing wastes. Vast volumes of iodine waste waters are stored at various places worldwide, e.g. at the Hanford site (a former plutonium production site in Washington USA) because of the lack of a suitable treatment method (Zhang et al. 2013). The geosphere or the conventional synthetic materials used for the purification of other radioactive contaminants do not efficiently adsorb the different species of iodine (Li et al. 2018).

The complex chemistry of iodine makes the waste treatment difficult. Iodine has multiple stable redox states with different chemical and physical properties. For example, iodine (I_2) can occur as gas and iodide (I^-) and iodate (IO_3^-) are usually present as dissolved ions in solution. (Kaplan et al. 2014) IO_3^- is the main species in aqueous solution and oxidizing conditions, whereas I^- prevails in more reducing environments. Molecular iodine, I_2 , is a major species only in low pH and over a narrow E_h range (Moore et al. 2019). In addition to the inorganic species, iodine also reacts readily with organic compounds producing organo-iodine compounds with a wide range of chemical characteristics (Andersen et al. 2002). The diversity of

iodine speciation and the fact that iodine can be present at several redox states simultaneously make a development of a universal iodine removal material hard or even impossible. Therefore, different removal strategies are required for the different iodine species.

The iodide decontamination has been successfully demonstrated with silver-containing materials. Activated carbons (Asmussen et al. 2016; Ho and Kraus 1981; Hoskins et al. 2002; Karanfil et al. 2005), zeolites (Asmussen et al. 2016; Faghihian et al. 2002) and metal oxides with silver impregnation have been demonstrated to successfully remove the iodide, presumably by formation of scarcely soluble AgI ($K_{sp} = 8.5 \times 10^{-17}$). In addition, hydrotalcites (Levitskaia et al. 2016) and organoclays (Bors et al. 2000) have shown significant capability of removing iodide. The iodate removal methods studied previously include hydroxyapatites (Campayo et al. 2011; Coulon et al. 2014), sulphur-containing minerals (Strickert et al. 1980), hydrotalcites (Levitskaia et al. 2016; Liang and Li 2007; Toraiishi et al. 2002), zero-valent and sulphur-modified iron (Lawter et al. 2018) and co-precipitation with calcite (Truex et al. 2017; Zhang et al. 2013). Despite the studies, the removal of iodate in the industrial scale still remains a difficult task and further studies as well as novel approaches are required.

Zirconium oxide (ZrO_2 , also known as zirconia) and its doped (e.g. Y, Ca, Ce or Sb) derivatives have a versatile range of favourable properties like toughness, high physical and chemical stability, low solubility in water, and high ionic conductivity, which are utilized in a wide range of applications, including catalysts (Shao et al. 2010), gas sensors (Borhade et al. 2018), ceramics (Zhang et al. 2014) and fuel cells (Malolepszy et al. 2015).

ZrO_2 has different crystalline and non-crystalline structures: the three crystalline (monoclinic, tetragonal and cubic) and the amorphous phase are stable at low pressures. The stability and prevalence of the different structures depend on many factors like the concentration and nature of dopants, crystallite size and synthesis conditions. (Graeve 2008) ZrO_2 is also known for both cation and anion-exchange properties (Singh and Tandon 1977; Veselý and Pekárek 1972). Antimony as dopant can affect the adsorption performance of ZrO_2 in many ways. It might be involved in redox reactions depending on the adsorbate element and the oxidation state (III or V) of antimony used as a dopant. Most importantly, the introduction of trivalent dopant ion, such as antimony, to the crystal structure of ZrO_2 creates crystal defects increasing the number of the oxygen vacancies (Graeve 2008). The latter could enhance the interaction of the material with oxygen-containing substances.

Indeed, pure and doped zirconium oxides have been widely studied for the decontamination of antimony (Lönrot et al. 2019; Paaajanen et al. 2019), technetium (Lönrot et al. 2020), fluoride (Dou et al. 2012; He et al. 2014),



phosphorus (Cui et al. 2012; Liu et al. 2008), arsenic (Cui et al. 2012; Zheng et al. 2011, 2012) and mercury (Mishra et al. 1996), for instance. Both pure and antimony-doped hydrous zirconium oxide have shown an excellent performance for the separation of different contaminant oxyanions, e.g. Sb and Tc (Lönnrot et al. 2019, 2020; Paaanen et al. 2019).

Iodine, similar to antimony and technetium, is present as an oxyanion in oxidizing conditions, but its adsorption properties on zirconium oxides have not been extensively studied. This study aims to fill that gap. The effect of the solution matrix (different competing ions in different concentrations, pH) and the uptake kinetics were studied by batch experiments. In addition, the application of the ZrO₂-based material in water treatment was demonstrated using ¹²⁵IO₃⁻ and ¹²⁷IO₃⁻ spiked simulant solution in dynamic column experiments.

The main laboratory experiments of this study were performed at the Radiochemistry unit at the Department of Chemistry, the Faculty of Science, the University of Helsinki, Finland, between the years 2019 and 2020. The synchrotron experiments were performed at BL22-CLÆSS beamline of the ALBA synchrotron light source, at Barcelona, Spain.

Materials and methods

Chemicals

All reagents were of analytical grade (Alfa Aesar, Sigma-Aldrich, Riedel de Haen) and used without further purification. The radioactive Na¹²⁵I tracer was purchased from PerkinElmer. Solutions were made by dissolving solids in grade 1 deionized water (18.2 MΩ cm at 25 °C, Milli-Q® Merck Millipore).

The test solutions used in the experiments consisted of simple solutions containing single competing anion prepared by dissolving appropriate amount of H₃BO₃ in the case of the borate, or sodium salts of the other corresponding anions (NaCl, NaNO₃, Na₂SO₄) in water. In addition to the simple solutions, also a more complex water simulant solution representing chloride containing process water (Table 1) was used in the batch experiments and in a single column experiment. The solution was prepared by dissolving Na, Ca or Mg salts of the anions and pH of the solution was finally adjusted to 7.0 with 1 M NaOH (Na⁺ from this step is also included in the values described in Table 1).

Synthesis of materials

ZrO₂ with and without antimony doping was synthesized with a precipitation method. First, in the case of ZrO₂ 100 g

Table 1 The composition of simulant process water solution used in some of the batch and column experiments

Component	Concentration (mM)
SO ₄ ²⁻	2.8
Cl ⁻	56.4
NO ₃ ⁻	6.6
Na ⁺	58.7
Ca ²⁺	1.2
Mg ²⁺	3.3

of zirconium basic carbonate (Alfa Aesar) was carefully dissolved in 1 L of 6 M HNO₃ under vigorous stirring using a mechanical stirrer. In the case of Zr(Sb)O₂, 45 g of ZrCl₄ (Riedel de Haen) and 2 g of SbCl₃ (Sigma-Aldrich) were used as the starting materials and they were dissolved in 2 L of 3 M HCl.

Next, approximately 1200 ml of 6 M NH₃ solution was slowly added to both beakers until pH reached 7.8 and white precipitate was formed. The precipitate was let to settle for overnight, and white precipitate and clear supernatant were separated. The precipitate was washed with deionized water until the conductivity of the supernatant was less than 4.0 mS/cm. Finally, the supernatant was discarded, and the slurry was dried in an oven at 70 °C for three days. The dried sample was ground to fine powder and sieved to particle size 74–149 μm.

Characterization

The surface morphologies of the materials coated with 4 nm Au–Pd sputtering were examined using Hitachi S4800 FE-SEM (field-emission scanning electron microscopy). The crystallinity was studied with powder X-ray diffraction (XRD) in the Bragg–Brentano geometry using a Pananalytical X'pert PW3710 MPD diffractometer, a PW3020 vertical goniometer and a Cu Kα radiation source (λ = 1.54056 Å, 40 kV and 40 mA).

Zeta potential of the materials was measured with Malvern Pananalytical Zetasizer Nano ZS. In these experiments, 20 mg of ZrO₂ or ZrSbO₂ ground fine powder and 10 ml of 10 mM NaNO₃ were mixed in a rotary mixer for 24 h before the measurement of the equilibrium pH and Zeta potential. Separate samples were prepared, and their pH was individually adjusted using diluted HCl or NaOH solutions.

Measurement of iodate concentration

Two different iodate probes were used in the experiments of this study: radioactive ¹²⁵IO₃⁻ and stable ¹²⁷IO₃⁻. In the case of experiments with radioactive ¹²⁵IO₃⁻ tracer, 5 ml of filtered solutions in polyethylene vials was measured with Wallac 1480 Wizard 3" automated NaI-scintillation γ-detector.



For the experiments with non-radioactive $^{127}\text{IO}_3^-$, 1 ml of filtered solution in a glass HPLC vial was analysed for iodide/iodate concentrations with an anion-exchange chromatography column (Dionex AS11 4×250 mm analytical column and AG11 4×50 mm guard column) attached to an Agilent 1260 Infinity quaternary pump and autosampler HPLC-system connected to an Agilent 7800 ICP-MS via direct connection between the column and ICP nebulizer. 50 mM sodium hydroxide (NaOH) was used as an eluent with a flow rate of 0.8 ml/min. The ICP-MS was driven in the no-gas mode. The dissolution of CO_2 from the ambient laboratory air was prevented by a constant Ar gas bubbling to the eluent container. The two main species of iodine I^- and IO_3^- were separated based on their retention times, first determined with standard solutions prepared from KI and KIO_3 , and the concentrations were calculated from the chromatogram peak areas using external standards on the concentration range from 0 to $200 \mu\text{g L}^{-1}$ for both iodine species. The stability of the instrument was followed using quality control ($5 + 5$ and $50 + 50 \mu\text{g L}^{-1}$ of total iodine $\text{I}^- + \text{IO}_3^-$) and blank samples. The retention times were 120 s for IO_3^- and 360 s for I^- and they remained stable during the analysis period. A limit of detection (LOD) for HPLC-ICP-MS system was $0.5 \mu\text{g L}^{-1}$ and $0.2 \mu\text{g L}^{-1}$ for I^- and IO_3^- , respectively. A repeated injection method was used for LOD determination by measuring 8 replicates of $1 \mu\text{g L}^{-1}$ of I^- and IO_3^- calibration standard and using a calculation procedure described the literature (Wells et al. 2011).

The speciation of iodine was confirmed with two methods depending on whether radioactive $^{125}\text{IO}_3^-$ or non-radioactive $^{127}\text{IO}_3^-$ was used. For experiments with non-radioactive iodine, commercial $\text{K}^{127}\text{IO}_3$ was used as the tracer without any treatment. In addition, the speciation was confirmed using HPLC-ICP-MS. However, because the radioactive tracer was in the form of Na^{125}I , the oxidation of iodide to iodate was needed. In order to obtain $^{125}\text{IO}_3^-$ solutions, an appropriate volume of NaOCl solution was added to obtain 2×10^{-4} M NaOCl concentration in 10 mM NaOH and the solution was let stand for at least 24 h before use. The speciation of $^{125}\text{IO}_3^-$ was confirmed with repeated simple batch experiments done for tracer solutions where silver-impregnated activated carbon (Silcarbon Aktivkohle GmbH, Germany) was used to quantify the iodate fraction. The procedure has been previously validated for the alteration and separation of the oxidation states of iodine (Suorsa et al. 2020).

Batch ion exchange experiments

To assess the potential of zirconium oxides on iodate uptake, the combined effect of different competing ions in different pH's and concentrations was studied with batch experiments.

The sample preparation in all batch experiments was similar: 20 ± 1 mg of ground material was weighed to a polyethylene vial, 10 ml of appropriate test solution was pipetted, and pH was adjusted by adding appropriate volume of NaOH or HCl and finally either $^{125}\text{IO}_3^-$ or $^{127}\text{IO}_3^-$ was added as tracer. The samples were equilibrated for 24 ± 2 h and solid and liquid phases were separated by centrifuging (2100 G, 10 min) followed by filtering with a $0.2 \mu\text{m}$ filter (PVDF LC, Arcodisc, Gellman Sciences). The filtered solution was either put to a 10 mL polyethylene vial (^{125}I) or a glass HPLC vial (^{127}I). The equilibrium pH of remaining supernatant was measured using Ross combined electrode. The determination of iodine concentration was done with NaI-scintillation γ -detector (^{125}I) or HPLC-ICP-MS (^{127}I) depending on whether the radioactive or stable isotope of iodine was used in the particular experiment.

The effect of competing ions to iodate adsorption was tested by using 10 mM solutions of different anions (Cl^- , NO_3^- , $\text{B}(\text{OH})_4^-$, SO_4^{2-}) as a function of pH in the range 3–10. The effect of concentration of ions was screened at single pH value using different concentrations (1, 10 and 100 mM). The experiments with single competing ion were separately done with the radioactive $^{125}\text{IO}_3^-$. In addition, a pH series with simulant solution (see Table 1) containing several components was done with non-radioactive $^{127}\text{IO}_3^-$. The latter was done to assess the effect of a more complex matrix as well as the potential difference between $^{125}\text{IO}_3^-$ and $^{127}\text{IO}_3^-$ possibly caused by the concentration or speciation differences. The radioactivity of carrier-free ^{125}I was between 100–250 Bq per 10 ml sample corresponding to concentrations on the scale $\sim 10^{-13}$ M. With non-radioactive ^{127}I , the concentrations were 8×10^{-7} M.

The distribution coefficients, K_d 's, in the batch experiments were calculated by Eq. 1:

$$K_d = \frac{c_i - c_f}{c_f} \times \frac{V}{m} \quad (1)$$

where c_i = initial concentration of iodate in the solution; c_f = final concentration of iodate in the solution; V = volume of solution in mL; and m = mass of material in g.

The error calculations are represented in SI.

Column experiments

Dynamic column experiments were done to test the zirconium oxide materials iodate uptake properties in more practical setup. Three sets of column experiments were done: first experiment with solution containing only 10 mM $^{127}\text{KIO}_3$ to see maximum apparent capacity, second experiment with 10 mM NaNO_3 , 1 mM KIO_3 and $^{125}\text{IO}_3^-$ as tracer to see the effect of weakly competing anion and last experiment with more complex simulant solution (Table 1) demonstrating the uptake properties in more realistic conditions from the waste management

point of view. Two first experiments were done for both ZrSbO_2 and ZrO_2 , the last experiment only with ZrSbO_2 .

Approximately 0.5 g (1 g in the case of third experiment with simulant solution) of the sieved material (74–149 μm) was loaded by pipetting with a small volume of 10 mM NaNO_3 to a low-pressure borosilicate glass column with a diameter of 0.7 cm and a porous polymer bed support at the bottom (Econo-Column®. Bio-Rad Laboratories, Inc.). Two different approaches were used for the probing of the breakthrough: non-radioactive $^{127}\text{IO}_3^-$ tracer and radioactive $^{125}\text{IO}_3^-$. The specifications of the individual column experiment sets are described in detail in Table 2.

$^{125}\text{IO}_3^-$ or $^{127}\text{IO}_3^-$ spiked simulant solution was pumped through the column bed (volume ~0.6 ml for the experiments 1 and 2, ~1.2 ml for column experiment 3 with simulant solution) with a flow rate of 10 bed volumes per hour. For the column experiment 1, only the total concentration of iodate and pH of effluent and eluent were measured, i.e. no individual fractions were collected. In the case of column experiments 1 and 2, the automated fraction collector was used to collect samples with the interval between one and two hours and samples were measured for iodate concentration and pH. In addition, the feed solutions were inspected regularly for iodate concentration and pH to make sure no changes in speciation, for example, had occurred before the contact with the materials.

The I K-edge XANES (X-ray absorption near edge structure) spectra of the IO_3^- loaded ZrO_2 and ZrSbO_2 (from Column experiment 1) were measured at BL22-CLÆSS beamline (Simonelli et al. 2016) of the ALBA synchrotron light source, Barcelona, Spain. The loaded column beds were moved to separate vials and washed two times by mixing with 5 mL of deionized water, followed by centrifugation (2100 G, 10 min) and removal of supernatant. After the wash, the samples were dried in 70 °C for overnight. The samples and the reference materials were homogenized with a mortar and pestle, and approximately 50 mg of sample (less in the case of references) was mixed with 150 mg of cellulose and pressed into pellets. The samples were measured in transmission mode inside a He-cryostat. The collected spectra were analysed and merged with Athena software (Ravel and Newville 2005). The XANES spectra of the samples were compared with KIO_3 , I_2 and KI as reference materials.

Table 2 The specifications of different column experiments performed during the study

Column experiment	Materials	Solution	Feed pH	IO_3^- probe	IO_3^- analysis method
1	ZrO_2 & ZrSbO_2	10 mM KIO_3	6.0	$^{127}\text{IO}_3^-$	HPLC-ICP-MS
2	ZrO_2 & ZrSbO_2	10 mM NaNO_3 + 1 mM KIO_3	6.0	$^{125}\text{IO}_3^-$	NaI-scintillation γ -detector
3	ZrSbO_2	Simulant solution (Table 1) + 4 μM KIO_3	7.0	$^{127}\text{IO}_3^-$	HPLC-ICP-MS

Results and discussion

Characterization

The synthesized materials were examined using XRD for their crystallinity (Fig. 1a), SEM for their morphology (ZrSbO_2 : Fig. 1b, see Supplementary Information (SI) Fig. 1 for ZrO_2) and electrophoretic light scattering for the isoelectric point (see SI Fig. 2). XRD of the zirconium oxide materials shows a broad peak located at 2θ of 30° making the determination of the crystal structure impossible. For both materials, the XRD and SEM measurements indicate the large aggregates of poorly crystalline zirconia. This kind of a structure is optimal for practical column use due to the low flow resistance and fast adsorption on the edge surfaces. Similar ZrO_2 syntheses in our previous studies yield materials with high surface area (Lönnrot et al. 2019).

The isoelectric points of the materials were determined by measuring Zeta potential in the pH range 4–10 (see SI Fig. 2) and the values are approximately 7.5 for both materials which agree with the published values in literature where the values of pH 3–8, usually around 7, have been reported (de Kretser and Scales 2008; Leong et al. 1995; Lönnrot et al. 2019; Schultz et al. 1993). The surface charge determines whether the anionic or cationic ions are attracted making it an important factor governing the uptake process.

Adsorption kinetics

The kinetics of iodate uptake was studied for both materials to see how fast uptake reaction proceeds to equilibrium (see SI for the graph). From the start, both materials showed a similar trend, and the adsorption reaches over 99.5% after 60 min. We suspect that reaction kinetics is fast because IO_3^- does not have to diffuse inside the crystalline structure; instead, the adsorption occurs on the crystallite surfaces.

Effect of pH and competing ions on the adsorption

The effect of pH was studied in the range between 3 and 10 with a series of batch experiments done with different competing ions (Cl^- , NO_3^- , SO_4^{2-} and B(OH)_4^-) in a concentration of 10 mM. The results are shown as a mean of



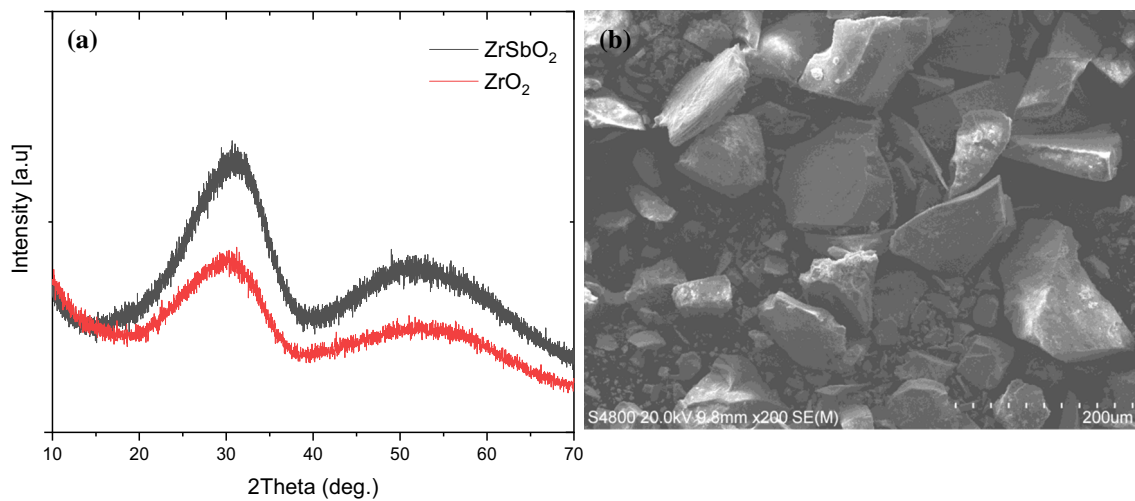


Fig. 1 Powder XRD patterns (a) of ZrO_2 (lower red line) and ZrSbO_2 (upper black line) materials and FE-SEM picture of ZrSbO_2 (b). See SI for the FE-SEM picture representing similar granules of ZrO_2

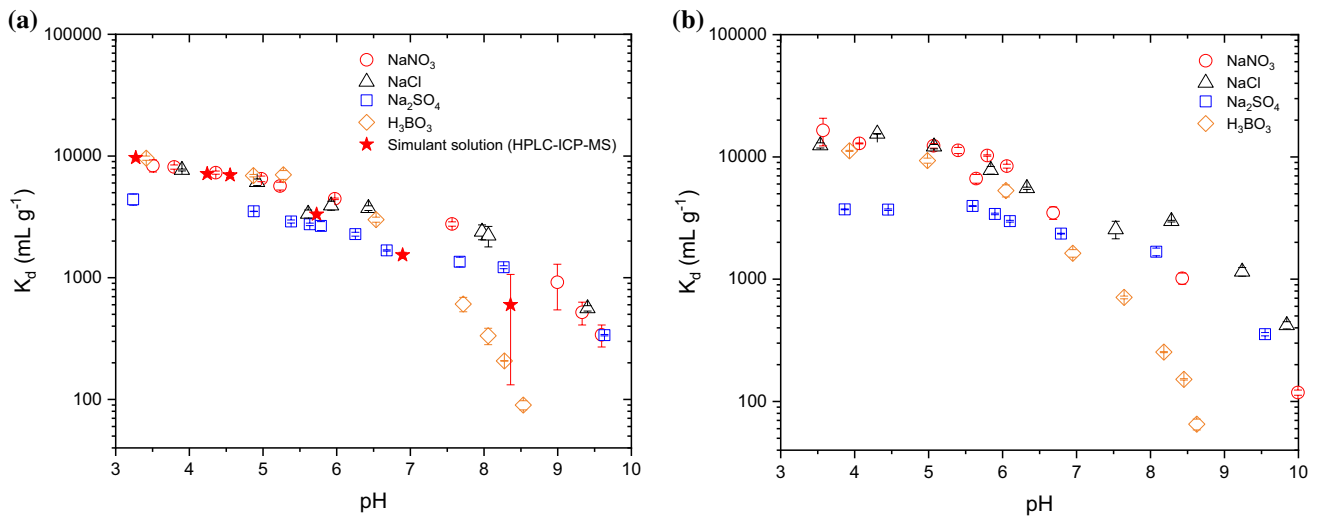


Fig. 2 The distribution coefficient (K_d) of IO_3^- for Zr(Sb)O_2 (a) and ZrO_2 (b) as a function of pH in with different competing ions in concentration of 10 mM

parallel samples ($n=2$), the error bars represent the standard deviation of the parallel samples ($n=2$) and are included in the figure but are not showing for all of the data points as they are less than the size of the markers. Both ZrSbO_2 and ZrO_2 show a similar uptake trend for IO_3^- as the function of pH (Fig. 2): the K_d values are the highest at low pH ($10,000 \text{ mL g}^{-1}$) and decrease as function of pH (100 mL g^{-1}). A clearly visible decrease in uptake is observed for all the ions at pH 8. This is most likely associated with the isoelectric point of ZrO_2 and ZrSbO_2 which lie within this range (see SI Fig. 2). Above this point, the surface charges of the materials turn negative causing the repulsion of negatively charged ions and inhibiting the adsorption process. From all

the ions, SO_4^{2-} has the most dramatic effect on IO_3^- uptake. The uptake of IO_3^- in SO_4^{2-} solution was notably less at low pH compared with other competing ions. At low pH, the divalent charge of sulphate strongly affects the iodate uptake. At pH's closer and above the isoelectric points, the differences in uptake are significantly smaller apart from borate that has changed its speciation from neutral B(OH)_3 to negatively charged B(OH)_4^- . It is suggested that the uptake of iodate at high pH is other than traditional anion uptake (rather uptake to defect sites at the material surface). In addition, SO_4^{2-} may react with the hydroxyl groups in zirconia causing the sulphonation of the surface (Chen et al. 1993; Deshmane and Adewuyi 2013). Compared with

SO_4^{2-} , the uptake of IO_3^- is significantly higher in the case of NO_3^- and Cl^- as competing ions. In borate solution, the IO_3^- uptake is at the same level with the latter at low pH (<6), but at higher pH a significant drop in the IO_3^- uptake was observed most likely due to the speciation change of borate. The anionic $\text{B}(\text{OH})_4^-$ becomes thermodynamically stable above pH 7 and competes more with IO_3^- compared with neutral $\text{B}(\text{OH})_3$ which is the only species in low pH.

The effect of concentration (1–100 mM) of competing ions Cl^- , NO_3^- , SO_4^{2-} was tested (Fig. 3) for both ZrO_2 and ZrSbO_2 but only at pH 4, where the IO_3^- uptake should be rather optimal based on the pH effect studies conducted in this study (Fig. 2). Figure 3 represents the distribution coefficients calculated as a mean of the parallel samples ($n=3$). The error bars representing the standard deviation of the parallel samples are included in the figure but are not showing as they are less than the size of the markers. At the tested conditions, the difference in Cl^- and NO_3^- concentrations did not show any effect on IO_3^- uptake as the K_d 's remained high (> 10,000 ml/g) over the concentration range. In the case of borate, pH 8 was used because the anionic species of borate are not thermodynamically stable in pH 4. For $\text{B}(\text{OH})_4^-$ at pH 8, the decrease of IO_3^- uptake as the function of borate concentration is dramatic: 100-fold from 10 000 to 100 ml/g for ZrSbO_2 and even more in the case of

ZrO_2 . The adsorption behaviour of IO_3^- in the presence of $\text{B}(\text{OH})_4^-$ resembles the typical uni–uni ion exchange reaction, but it should be noted that pH values are close to the PZC and were measured with a pH electrode and therefore are not accurate enough for a precise determination of exchange reaction. Compared with borate, the rise of SO_4^{2-} concentration affected the uptake less: K_d values drop ten-fold from 10 000 ml/g at 1 mM to almost 1 000 ml/g at 100 mM. This does not agree with typical 1:2 ion exchange between SO_4^{2-} and IO_3^- and the role of other uptake processes, like surface complexation, has to be considered for IO_3^- uptake besides ion exchange.

As the IO_3^- adsorption is unaffected by increasing ionic strength in the case of NO_3^- or Cl^- , it would indicate that the adsorption is not, at least solely, due the ion exchange. The rising SO_4^{2-} and $\text{B}(\text{OH})_4^-$ concentrations have a strong effect on IO_3^- adsorption which would indicate that they are competing for the same sites with the latter at the corresponding conditions.

Column experiments

The series of column experiments were performed to assess the suitability of ZrO_2 and ZrSbO_2 in a more practical column set-up. Three sets of column experiments were done (Table 3): first experiment with solution containing only

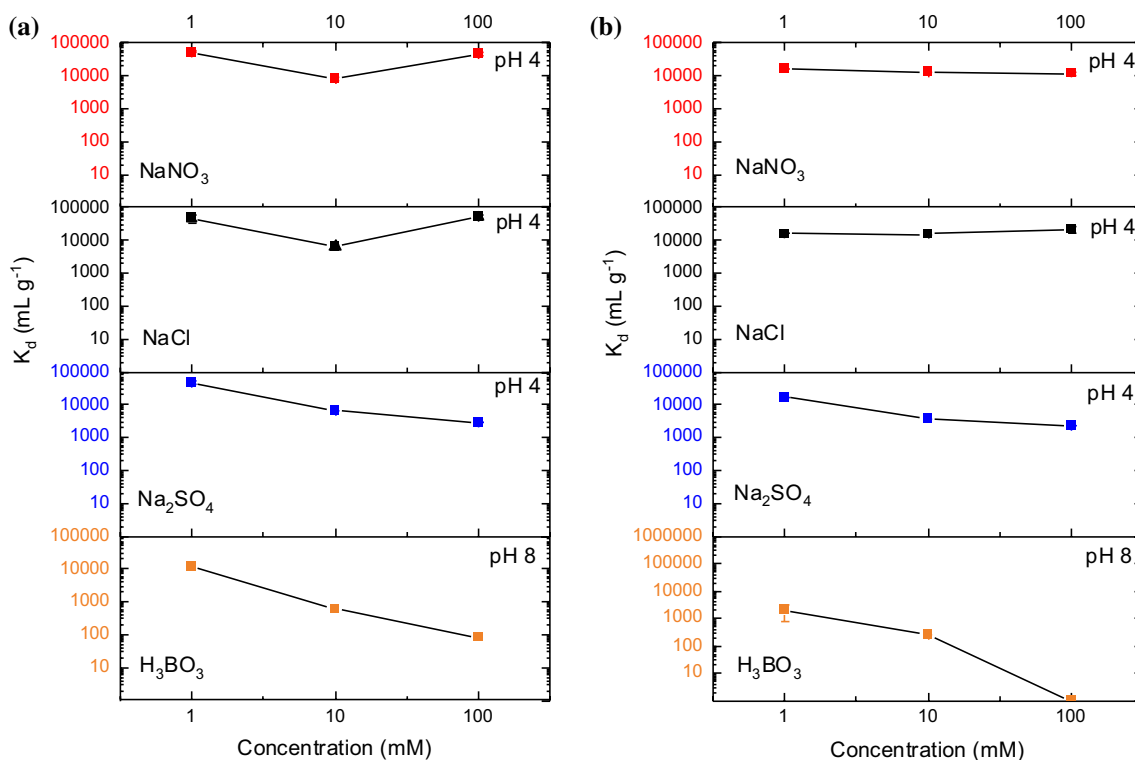


Fig. 3 The distribution coefficient (K_d) of IO_3^- for Zr(Sb)O_2 (a) and pure ZrO_2 (b) as concentration 1–100 mM of different competing ions



10 mM $^{127}\text{KIO}_3$ (to see maximum apparent capacity), second experiment with 10 mM NaNO_3 , 1 mM KIO_3 traced with $^{125}\text{IO}_3^-$ (as an iodate tracer for accurate and simple measurements) and third experiment with more complex simulant solution (Table 1), demonstrating the performance under more realistic conditions.

In simple KIO_3 solution, both materials showed similar apparent capacities for iodate: ZrSbO_2 (3.5 mmol/g) performed slightly more efficiently compared with ZrO_2 (3.2 mmol/g). The feed pH was 6.0 and final pH 4.7 and 4.3 for ZrSbO_2 and ZrO_2 , respectively. The HPLC-ICP-MS (See SI for the example chromatograms) analysis did not show any changes in iodine oxidation state as only IO_3^- was observed in the eluent and no I^- or other iodine species were detected in effluent. In addition, the measured iodine K-edge XANES spectra of both ZrO_2 and ZrSbO_2 (Fig. 4) show the features characteristic to iodate, confirming that no redox changes occurred during the adsorption and iodine adsorbed to the materials as iodate.

In 10 mM NaNO_3 solution, the IO_3^- uptake performance was reduced for both materials. Like in the first set of column experiments, ZrSbO_2 (0.64 mmol/g) performed more efficiently compared with ZrO_2 (0.58 mmol/g). The breakthrough curves of IO_3^- in these experiments are presented in Fig. 5. The breakthrough curve shows highly symmetrical shape for ZrSbO_2 and the breakthrough started at approximately 500 BV's. For ZrO_2 , the breakthrough started at earlier stage after approximately 300 BV's. The complete breakthrough was achieved at the same stage for both materials at 700 BV's. The pH evolutions of the eluents were similar for both materials (Fig. 6). pH raised steadily from initial 2.5 to 4.0. At the same point when the actual breakthrough started (600 BV's), pH rose fast to 5.0. In general, the pH was slightly lower in the case of ZrSbO_2 compared with ZrO_2 at the corresponding points of the experiment.

The performance of ZrSbO_2 , which showed higher apparent capacity for IO_3^- in previous experiments, was also tested in a more complex solution (Table 1) to better assess its suitability for real applications (Fig. 7). The breakthrough of IO_3^- appeared after 1250 BV's, and the complete breakthrough was achieved at 2500 BV's. The apparent capacity

Table 3 The column experiments performed within the study

Material	Solution	Feed pH	Apparent IO_3^- capacity (mmol/g)
ZrO_2	10 mM KIO_3	6.0	3.18 ± 0.09
	10 mM NaNO_3 + 1 mM KIO_3	6.0	0.58 ± 0.01
ZrSbO_2	10 mM KIO_3	6.0	3.49 ± 0.17
	10 mM NaNO_3 + 1 mM KIO_3	6.0	0.64 ± 0.01
	Simulant solution (see Table 1)	7.0	0.0047 ± 0.0001

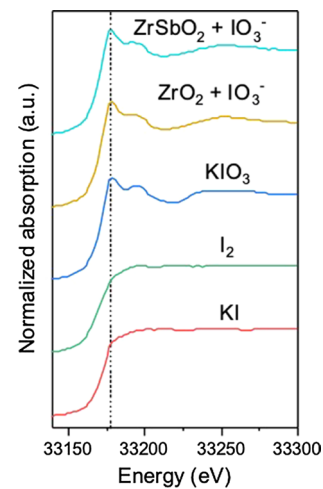


Fig. 4 Normalized I K-edge XANES spectra of the reference samples and zirconium materials loaded with IO_3^- (ZrO_2 : 3.2 mmol/g; ZrSbO_2 : 3.49 mmol/g)

in these conditions seems to be dramatically lower (approximately 5 $\mu\text{mol/g}$) compared with simpler solution in the previous column experiments. Most probably, this is because of the competition of other ions, especially divalent sulphate, which was also observed in the batch experiments. A steep rise in pH occurred at the same time with the breakthrough.

Altogether, the column experiments demonstrate that the IO_3^- apparent adsorption capacity is lowered from the ideal conditions due to competing anions. However, even at complex solution (Fig. 7) with a high excess of other ions (SO_4^{2-} and Cl^- to IO_3^- ratios 700 and 14,000, respectively) a selective removal of IO_3^- is achieved. The lower uptake in the column experiments with higher ionic strength can

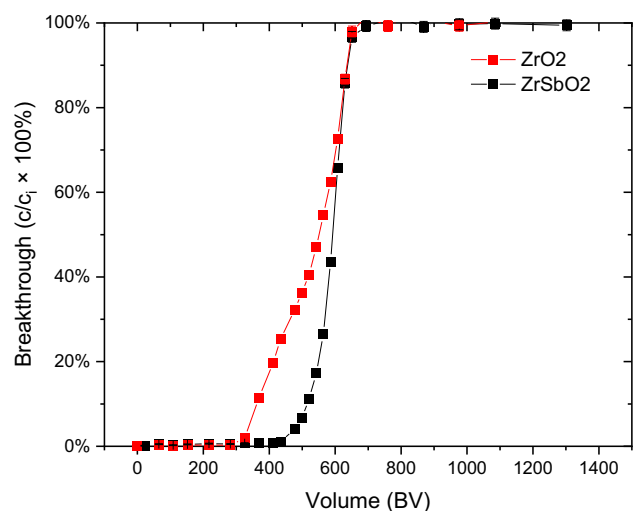


Fig. 5 Breakthrough of IO_3^- for ZrSbO_2 (black) and ZrO_2 (red) columns as the function of effluent volume in bed volumes. The error bars are not showing as they remain hidden behind the symbols

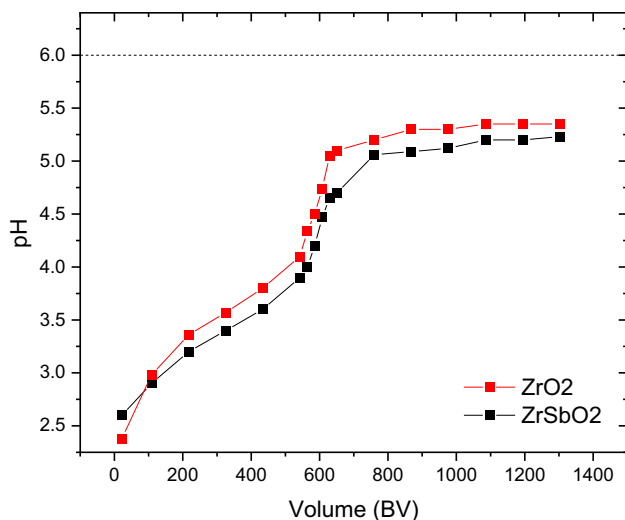


Fig. 6 pH values of effluent fractions from the column experiments done with 10 mM NaNO_3 . The dashed line shows the pH of the feed solution (6.0)

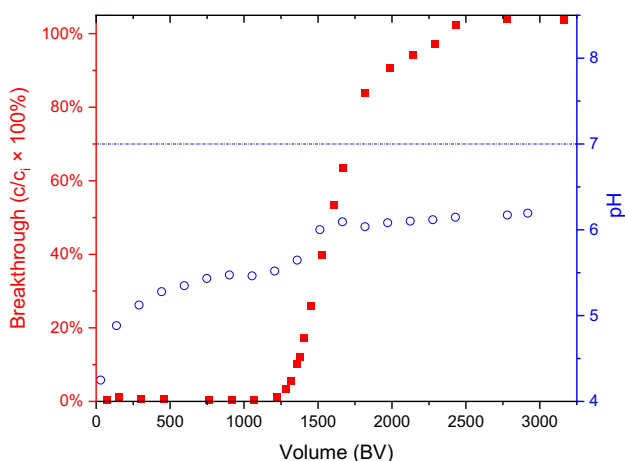


Fig. 7 Breakthrough of iodate (red squares, left axis) and pH of effluent (open blue circles and right axis) as in simulant solution. The dashed line shows the pH of the eluent (7.0)

be explained by the presence of two different adsorption sites for IO_3^- on the zirconium oxide materials with different adsorption mechanisms. This is supported by the results of the batch experiments (“Effect of pH and competing ions on the adsorption”) as the rising concentrations of Cl^- and NO_3^- do not affect the IO_3^- uptake at all, whereas higher SO_4^{2-} concentrations reduce it strongly. It is suggested that at ideal conditions without competing anions, IO_3^- is adsorbed to both selective and non-selective sites at the zirconium oxide materials. The introduction of NO_3^- or Cl^- lowers the removal performance because then IO_3^- is adsorbed mostly or only at the selective sites. In the presence of both Cl^- and SO_4^{2-} , the IO_3^- uptake is furthermore

decreased because the selective sites are shared between IO_3^- and SO_4^{2-} . Like suggested by the batch experiment results, SO_4^{2-} seems to compete for the IO_3^- selective sites indicating a similar adsorption mechanism. However, more detailed experiments are needed to verify the exact mechanism behind the adsorption of IO_3^- to the zirconium oxide materials.

Conclusion

This study altogether demonstrates the potential of zirconia-based materials on the selective removal of radioactive IO_3^- which currently is an unresolved task. The ZrO_2 and Sb-doped ZrO_2 exhibited the high apparent capacities of 3.2–3.5 mmol/g for IO_3^- in ideal conditions. More importantly, the materials showed high selectivity to IO_3^- as the uptake performance of the materials was unaffected by the large excess of competing NO_3^- or Cl^- ions (in batch). However, SO_4^{2-} and B(OH)_4^- lowered the iodate adsorption significantly in acidic and basic conditions, respectively. In addition, the apparent capacity was reduced from the ideal situation in more complex solutions due to the competition of the other anions from which the most important is SO_4^{2-} . This is most likely explained by its divalent charge and sulfonation of the material surface, which is a known phenomenon and observed in catalysis applications with zirconia. Although the apparent capacity was lowered significantly from the ideal in the presence of competing anions, the zirconia materials show potential for the remediation of radioactive wastes where the contaminants are often in trace concentration levels and the most important factor regarding the performance is the selectivity of the materials.

The pure and Sb-doped ZrO_2 performed both efficiently in IO_3^- removal, but the latter showed approximately 10% higher apparent capacity. It is likely that antimony disturbs the formation of ZrO_2 structure and produces more defects to the structure that are typically active adsorption sites for IO_3^- uptake. However, the exact role of antimony and the detailed uptake mechanism of IO_3^- require further investigation on the structure at the sorption site (preferably synchrotron-based XAS measurements) in order to optimize the removal performance of the materials. Consequently, competent zirconia adsorbent materials suitable for direct disposal could be developed for the present and forthcoming radioactive IO_3^- waste, which at the moment, lacks a specific removal method.

Supplementary Information The online version contains supplementary material available at <https://doi.org/10.1007/s13762-021-03487-9>.



Acknowledgements Financial support from the Doctoral Programme in Chemistry and Molecular Sciences (CHEMS) at the University of Helsinki is gratefully acknowledged. The X-ray absorption spectroscopy experiments were performed at BL22-CLAESS beamline at ALBA Synchrotron (Proposal no: 2020024264) with the collaboration of ALBA staff. The authors gratefully acknowledge the support of PhD Vlad Martin Diaconescu. The authors gratefully appreciate the help in batch and column experiments by Ms Susanna Heikkilä.

Funding Open access funding provided by University of Helsinki including Helsinki University Central Hospital. This work was funded by the Doctoral Programme in Chemistry and Molecular Sciences (CHEMS) at the University of Helsinki.

Data availability The additional data are contained in supplementary material.

Declarations

Conflict of interest The authors declare that they have no conflicts of interest.

Ethical approval This article does not contain any studies with human participants or animals performed by any of the authors.

Open Access This article is licensed under a Creative Commons Attribution 4.0 International License, which permits use, sharing, adaptation, distribution and reproduction in any medium or format, as long as you give appropriate credit to the original author(s) and the source, provide a link to the Creative Commons licence, and indicate if changes were made. The images or other third party material in this article are included in the article's Creative Commons licence, unless indicated otherwise in a credit line to the material. If material is not included in the article's Creative Commons licence and your intended use is not permitted by statutory regulation or exceeds the permitted use, you will need to obtain permission directly from the copyright holder. To view a copy of this licence, visit <http://creativecommons.org/licenses/by/4.0/>.


References

- Aldahan A, Alfimov V, Possnert G (2007) ^{129}I anthropogenic budget: major sources and sinks. *Appl Geochem* 22:606–618. <https://doi.org/10.1016/j.apgeochem.2006.12.006>
- Andersen S, Petersen S, Laurberg P (2002) Iodine in drinking water in Denmark is bound in humic substances. *Eur J Endocrinol* 147:663–670. <https://doi.org/10.1530/eje.0.1470663>
- Andersson M, de Benoist B, Rogers L (2010) Epidemiology of iodine deficiency: salt iodisation and iodine status. *Best Pract Res Clin Endocrinol Metab* 24:1–11. <https://doi.org/10.1016/j.beem.2009.08.005>
- Asmussen RM, Neeway JJ, Lawter AR, Wilson A, Qafoku NP (2016) Silver-based getters for ^{129}I removal from low-activity waste. *Radiochim Acta* 104:905–913. <https://doi.org/10.1515/ract-2016-2598>
- Borhade AV, Tope DR, Agashe JA (2018) Synthesis, characterization and gas sensing performance of nano-crystalline ZrO_2 , 5%Y/ ZrO_2 and Ag-5%Y/ ZrO_2 catalyst. *J Mater Sci Mater Electron* 29:7551–7561. <https://doi.org/10.1007/s10854-018-8747-3>
- Bors J, Dultz S, Riebe B (2000) Organophilic bentonites as adsorbents for radionuclides: I. Adsorption of ionic fission products. *Appl Clay Sci* 16:1–13. [https://doi.org/10.1016/S0169-1317\(99\)00041-1](https://doi.org/10.1016/S0169-1317(99)00041-1)
- Campayo L, Grandjean A, Coulon A, Delorme R, Vantelon D, Laurencin D (2011) Incorporation of iodates into hydroxyapatites: a new approach for the confinement of radioactive iodine. *J Mater Chem* 21:17609–17611. <https://doi.org/10.1039/C1JM14157K>
- Chen FR, Coudurier G, Joly JF, Vedrine JC (1993) Superacid and catalytic properties of sulfated zirconia. *J Catal* 143:616–626. <https://doi.org/10.1006/jcat.1993.1304>
- Coulon A, Laurencin D, Grandjean A, Cau Dit Coumes C, Rossignol S, Campayo L (2014) Immobilization of iodine into a hydroxyapatite structure prepared by cementation. *J Mater Chem A*. <https://doi.org/10.1039/C4TA03236E>
- Cui H, Li Q, Gao S, Shang JK (2012) Strong adsorption of arsenic species by amorphous zirconium oxide nanoparticles. *J Ind Eng Chem* 18:1418–1427. <https://doi.org/10.1016/j.jiec.2012.01.045>
- de Kretser RG, Scales PJ (2008) The effect of temperature on the yield stress of mineral suspensions. *J Colloid Interface Sci* 328:187–193. <https://doi.org/10.1016/j.jcis.2008.09.084>
- Deshmane VG, Adewuyi YG (2013) Mesoporous nanocrystalline sulfated zirconia synthesis and its application for FFA esterification in oils. *Appl Catal A* 462–463:196–206. <https://doi.org/10.1016/j.apcata.2013.05.005>
- Dou X, Mohan D, Pittman CU, Yang S (2012) Remediating fluoride from water using hydrous zirconium oxide. *Chem Eng J* 198–199:236–245. <https://doi.org/10.1016/j.cej.2012.05.084>
- Faghihian H, Ghannadi Maragheh M, Malekpour A (2002) Adsorption of radioactive iodide by natural zeolites. *J Radioanal Nucl* 254:545–550. <https://doi.org/10.1023/A:1021698207045>
- Graeve OA (2008) Zirconia. In: Shackelford JF, Doremus R (eds) *Ceramic and glass materials*. Springer, New York, USA, pp 169–197
- He J, Siah T, Paul Chen J (2014) Performance of an optimized Zr-based nanoparticle-embedded PSF blend hollow fiber membrane in treatment of fluoride contaminated water. *Water Res* 56:88–97. <https://doi.org/10.1016/j.watres.2014.02.030>
- Ho PC, Kraus KA (1981) Adsorption on inorganic materials-VIII: adsorption of iodide on AgCl-filled carbon. *J Inorg Nucl Chem* 43:583–587. [https://doi.org/10.1016/0022-1902\(81\)80507-6](https://doi.org/10.1016/0022-1902(81)80507-6)
- Hoskins JS, Karanfil T, Serkiz SM (2002) Removal and sequestration of iodide using silver-impregnated activated carbon. *Environ Sci Technol* 36:784–789. <https://doi.org/10.1021/es010972m>
- Hou X, Hansen V, Aldahan A, Possnert G, Lind OC, Lujanienė G (2009) A review on speciation of iodine-129 in the environmental and biological samples. *Anal Chim Acta* 632:181–196. <https://doi.org/10.1016/j.aca.2008.11.013>
- Hou X, Povinec PP, Zhang L, Shi K, Biddulph D, Chang C, Fan Y, Golser R, Hou Y, Jeřkovský M, Jull AJT, Liu Q, Luo M, Steier P, Zhou W (2013) Iodine-129 in seawater offshore Fukushima: distribution, inorganic speciation, sources, and budget. *Environ Sci Technol* 47:3091–3098. <https://doi.org/10.1021/es304460k>
- Kaplan DI, Denham ME, Zhang S, Yeager C, Xu C, Schwehr K, Li H, Ho Y, Wellman D, Santschi PH (2014) Radioiodine biogeochemistry and prevalence in groundwater. *Crit Rev Environ Sci Technol* 44:2287–2335. <https://doi.org/10.1080/10643389.2013.828273>
- Karanfil T, Moro E, Serkiz S (2005) Development and testing of a silver chloride-impregnated activated carbon for aqueous removal and sequestration of iodide. *Environ Technol* 26:1255–1262. <https://doi.org/10.1080/09593332608618595>
- Lawter AR, Garcia WL, Kukkadapu RK, Qafoku O, Bowden ME, Saslow SA, Qafoku NP (2018) Technetium and iodine aqueous species immobilization and transformations in the presence of strong reductants and calcite-forming solutions: remedial action implications. *Sci Total Environ* 636:588–595. <https://doi.org/10.1016/j.scitotenv.2018.04.240>

- Leong Y, Scales PJ, Healy TW, Boger DV (1995) Effect of particle size on colloidal zirconia rheology at the isoelectric point. *J Am Ceram Soc* 78:2209–2212. <https://doi.org/10.1111/j.1151-2916.1995.tb08638.x>
- Levitskaia TG, Chatterjee S, Arey BW, Campbell EL, Hong Y, Kovarik L, Peterson JM, Pence NK, Romero J, Shutthanandan V (2016) RedOx-controlled sorption of iodine anions by hydrotalcite composites. *RSC Adv* 6:76042–76055. <https://doi.org/10.1039/C6RA13092E>
- Li D, Kaplan DI, Sams A, Powell BA, Knox AS (2018) Removal capacity and chemical speciation of groundwater iodide (I^-) and iodate (IO_3^-) sequestered by organoclays and granular activated carbon. *Environ Radioact* 192:505–512. <https://doi.org/10.1016/j.jenvrad.2018.08.008>
- Liang L, Li L (2007) Adsorption behavior of calcined layered double hydroxides towards removal of iodide contaminants. *J Radioanal Nucl* 273:221–226
- Liu H, Sun X, Yin C, Hu C (2008) Removal of phosphate by mesoporous ZrO_2 . *J Hazard Mater* 151:616–622. <https://doi.org/10.1016/j.jhazmat.2007.06.033>
- Lönnrot S, Suorsa V, Paajanen J, Hatanpää T, Ritala M, Koivula R (2019) Submicron fibers as a morphological improvement of amorphous zirconium oxide particles and their utilization in antimonate (Sb(V)) removal. *RSC Adv* 9:22355–22365. <https://doi.org/10.1039/C9RA04211C>
- Lönnrot S, Paajanen J, Suorsa V, Zhang W, Ritala M, Koivula R (2020) Sb-doped zirconium dioxide submicron fibers for separation of pertechnetate (TcO_4^-) from aqueous solutions. *Sep Sci Technol*. <https://doi.org/10.1080/01496395.2020.1826967>
- Malolepszy A, Mazurkiewicz M, Stobinski L, Lesiak B, Kóvér L, Tóth J, Mierzwa B, Borodzinski A, Nitze F, Wågberg T (2015) Deactivation resistant Pd-ZrO₂ supported on multiwall carbon nanotubes catalyst for direct formic acid fuel cells. *Int J Hydrogen Energy* 40:16724–16733. <https://doi.org/10.1016/j.ijhydene.2015.08.048>
- Mishra SP, Singh VK, Tiwari D (1996) Radiotracer technique in adsorption study: part XIV. Efficient removal of mercury from aqueous solutions by hydrous zirconium oxide. *Appl Radiat Isot* 47:15–21. [https://doi.org/10.1016/0969-8043\(95\)00260-X](https://doi.org/10.1016/0969-8043(95)00260-X)
- Moore RC, Pearce CI, Morad JW, Chatterjee S, Levitskaia TG, Asmusen RM, Lawter AR, Neeway JJ, Qafoku NP, Rigali MJ (2019) Iodine immobilization by materials through sorption and redox-driven processes: a literature review. *Sci Total Environ*. <https://doi.org/10.1016/j.scitotenv.2019.06.166>
- Paajanen J, Lönnrot S, Heikkilä M, Meinander K, Kemell M, Hatanpää T, Ainassaari K, Ritala M, Koivula R (2019) Novel electroblowing synthesis of submicron zirconium dioxide fibers: effect of fiber structure on antimony (V) adsorption. *Nanoscale Adv* 1:4373–4383. <https://doi.org/10.1039/C9NA00414A>
- Ravel B, Newville M (2005) ATHENA, ARTEMIS, HEPHAESTUS: data analysis for X-ray absorption spectroscopy using IFEFFIT. *J Synchrotron Radiat* 12:537–541
- Schultz M, Grimm S, Burckhardt W (1993) The isoelectric point of pure and doped zirconia in relation to the preparation route. *Solid State Ionics* 63–65:18–24. [https://doi.org/10.1016/0167-2738\(93\)90080-M](https://doi.org/10.1016/0167-2738(93)90080-M)
- Shao Y, Xu Z, Wan H, Chen H, Liu F, Li L, Zheng S (2010) Influence of ZrO₂ properties on catalytic hydrodechlorination of chlorobenzene over Pd/ZrO₂ catalysts. *J Hazard Mater* 179:135–140. <https://doi.org/10.1016/j.jhazmat.2010.02.070>
- Simonelli L, Marini C, Olszewski W, Ávila Pérez M, Ramanan N, Guiler G, Cuartero V, Klementiev K (2016) CLÆSS: The hard X-ray absorption beamline of the ALBA CELLS synchrotron. *Cogent Phys* 3:1231987. <https://doi.org/10.1080/23311940.2016.1231987>
- Singh NJ, Tandon SN (1977) Hydrous zirconium oxide as an anion-exchanger. *Talanta* 24:459–461. [https://doi.org/10.1016/0039-9140\(77\)80129-X](https://doi.org/10.1016/0039-9140(77)80129-X)
- Strickert R, Friedman AM, Fried S (1980) The sorption of technetium and iodine radioisotopes by various minerals. *Nucl Technol* 49:253–266. <https://doi.org/10.13182/NT80-A32488>
- Suorsa V, Otaki M, Zhang W, Virkanen J, Koivula R (2020) A simple method for quantifying iodate and iodide fractions in solution using Ag-impregnated activated carbon. *J Radioanal Nucl*. <https://doi.org/10.1007/s10967-020-07061-4>
- Toraishi T, Nagasaki S, Tanaka S (2002) Adsorption behavior of IO_3^- by CO_3^{2-} - and NO_3^- -hydrotalcite. *Appl Clay Sci* 22:17–23. [https://doi.org/10.1016/S0169-1317\(02\)00108-4](https://doi.org/10.1016/S0169-1317(02)00108-4)
- Truex MJ, Lee BD, Johnson CD, Qafoku N, Szecsody JE, Kyle JE, Tfaily MM, Snyder M, Cantrell KJ, Saunders DL (2017) Conceptual model of iodine behavior in the subsurface at the Hanford site. *PNNL-24709 Rev 2*. <https://doi.org/10.2172/1419157>
- Veselý V, Pekárek V (1972) Synthetic inorganic ion-exchangers-I: hydrous oxides and acidic salts of multivalent metals. *Talanta* 19:219–262. [https://doi.org/10.1016/0039-9140\(72\)80075-4](https://doi.org/10.1016/0039-9140(72)80075-4)
- Wells G, Prest H, Russ C (2011) Signal, noise, and detection limits in mass spectrometry. Technical Note for Agilent Technologies Inc
- World Health Organization (2017) Guidelines for drinking-water quality: first addendum to the, 4th edn. World Health Organization, Geneva
- Zhang S, Xu C, Creeley D, Ho Y, Li H, Grandbois R, Schwehr KA, Kaplan DI, Yeager CM, Wellman D (2013) Iodine-129 and iodine-127 speciation in groundwater at the Hanford site, US: iodate incorporation into calcite. *Environ Sci Technol* 47:9635–9642. <https://doi.org/10.1021/es401816e>
- Zhang R, He R, Zhou W, Wang Y, Fang D (2014) Design and fabrication of porous ZrO₂/(ZrO₂ + Ni) sandwich ceramics with low thermal conductivity and high strength. *Mater Des* 1980–2015(62):1–6. <https://doi.org/10.1016/j.matdes.2014.05.006>
- Zheng Y, Zou S, Nanayakkara KGN, Matsuura T, Chen JP (2011) Adsorptive removal of arsenic from aqueous solution by a PVDF/zirconia blend flat sheet membrane. *J Membr Sci* 374:1–11. <https://doi.org/10.1016/j.memsci.2011.02.034>
- Zheng Y, Yu L, Wu D, Paul Chen J (2012) Removal of arsenite from aqueous solution by a zirconia nanoparticle. *Chem Eng J* 188:15–22. <https://doi.org/10.1016/j.cej.2011.12.054>
- Zimmermann MB, Andersson M (2012) Update on iodine status worldwide. *Curr Opin Endocrinol Diabetes Obes*. <https://doi.org/10.1097/MED.0b013e328357271a>
- Zimmermann MB, Boelaert K (2015) Iodine deficiency and thyroid disorders. *Lancet Diabetes Endocrinol* 3:286–295. [https://doi.org/10.1016/S2213-8587\(14\)70225-6](https://doi.org/10.1016/S2213-8587(14)70225-6)



Authors and Affiliations

V. Suorsa¹  · M. Otaki¹ · J. Virkanen² · R. Koivula¹

¹ Radiochemistry Unit, Department of Chemistry, University of Helsinki, A.I. Virtasen aukio 1, 00014 Helsinki, Finland

² Department of Geosciences and Geography, University of Helsinki, Gustaf Hällströmin katu 2, 00014 Helsinki, Finland

